Structure of Offshore Flow

DEAN VICKERS AND L. MAHRT

College of Oceanic and Atmospheric Sciences, Oregon State University, Corvallis, Oregon

JIELUN SUN

National Center for Atmospheric Research, Boulder, Colorado

TIM CRAWFORD

NOAA/FRD, Idaho Falls, Idaho

(Manuscript received 25 April 2000, in final form 1 September 2000)

ABSTRACT

The horizontal and vertical structure of the mean flow and turbulent fluxes are examined using aircraft observations taken near a barrier island on the east coast of the United States during offshore flow periods. The spatial structure is strongly influenced by the surface roughness and surface temperature discontinuities at the coast. With offshore flow of warm air over cool water, the sea surface momentum flux is large near the coast and decreases rapidly with increasing offshore distance or travel time. The decrease is attributed to advection and decay of turbulence from land. The rate of decrease is dependent on the characteristic timescale of the eddies in the upstream land-based boundary layer that are advected over the ocean. As a consequence, the air–sea momentum exchange near the coast is influenced by upstream conditions and similarity theory is not adequate to predict the flux.

The vertical structure reveals an elevated layer of downward momentum flux and turbulence energy maxima over the ocean. This increase in the momentum flux with height contributes to acceleration of the low-level mean wind. In the momentum budget, the vertical advection term, vertical flux divergence term, and the horizontal pressure gradient term are all of comparable magnitude and all act to balance large horizontal advection. An interpolation technique is applied to the aircraft data to develop fetch–height cross sections of the mean flow and momentum flux that are suitable for future verification of numerical models.

1. Introduction

In quasi-stationary atmospheric flow over a homogeneous surface, Monin–Obukhov similarity theory and bulk flux formula have successfully predicted turbulent surface fluxes over the sea (e.g., Fairall et al. 1996; Högström 1996). Here quasi-stationary means that the total time rate of change of turbulent quantities is small compared to production and dissipation terms. However, in regions of significant surface heterogeneity, such as near coastlines, advection by the mean wind and vertical flux divergence can become significant. In this case, a well-defined surface layer may not exist, and similarity theory will be inadequate due to a dependence of the fluxes on upstream conditions.

With offshore flow, the turbulence advected from land must adjust to the new aerodynamically smoother sea surface and new surface temperature. A conceptual model of this adjustment is internal boundary layer theory (Garratt 1990). The internal boundary layer (IBL) is the region near the surface where the flow is directly influenced by the new underlying surface. While unstable IBLs (e.g., cool air over warm water) have a well-defined convective growth mechanism due to the surface heat flux, the stable case is more complex and less well understood. In the stable case, the residual land-based turbulence advected downwind above the stable IBL may be stronger than the turbulence within the IBL, leading to an increase in turbulence kinetic energy (TKE) with height. This occurs despite the fact that the residual turbulence generated over land decays through dissipation as it is advected over the water. This stable case is not described by traditional IBL theory (Mahrt et al. 2001).

Advection and decay of convective turbulence were studied by Nieuwstadt and Brost (1986) by abruptly switching off the upward surface heat flux in a large-

Corresponding author address: Dean Vickers, College of Oceanic and Atmospheric Sciences, Oceanography Admin. Bldg. 104, Oregon State University, Corvallis, OR 97331-5503.
E-mail: vickers@oce.orst.edu

eddy simulation model. They found that the relevant scaling parameters of the decay of TKE were the convective velocity scale w_* and the mixed layer depth h. Sorbjan (1997) extended the modeling approach by imposing a gradual rather than a sudden time change in the surface heat flux. Studies reviewed in Monin and Yaglom (1975) suggest that the integral length scale of decaying turbulence increases with time due to finescale eddies decaying first. The influence of advection of covariances by the mean wind on the measured flux is sometimes viewed in terms of the flux footprint approach. With strong winds, the footprint may extend a considerable distance in the upwind direction (Horst and Weil 1994). This situation is further complicated by the fact that the eddies associated with the land-based fluxes decay through dissipation and that the momentum fluxes are influenced by pressure fluctuations, neither of which are included in footprint theory.

In the coastal region, the sea surface momentum flux can also be influenced by shoaling waves and young growing gravity wave fields on the ocean surface. With shoaling waves, wave breaking and wave steepening can augment the momentum flux (Banner 1990). Wind–wave interaction leading to development of new (young) waves can augment the momentum flux compared to conditions with older wave fields that are more in equilibrium with the wind (Geernaert et al. 1987; Donelan 1990).

Numerous authors have reported evidence of marine low-level jets in offshore flow (e.g., Smedman et al. 1993 and references therein). They propose that the jet is formed due to an inertial oscillation caused by frictional decoupling from the surface when warm air flows over cooler water. The decoupling occurs because the turbulence near the surface collapses partly due to buoyancy destruction. Smedman et al. (1993) make an analogy between the spatial structure of the marine jet and the more well known nocturnal jet over land.

In this work, we investigate the spatial structure of the mean flow, momentum flux, heat flux, and TKE in the first 10 km offshore as land-based turbulence is advected over the water, influenced by the new smoother sea surface, and modified by the stratification. For stable conditions, we relate the timescale associated with the observed decrease in the sea surface momentum flux with travel time from the coast to a decay timescale characteristic of the turbulence in the boundary layer over land. Individual terms in the equation of motion for the mean wind are examined. The data description and analysis methods are discussed in the next section. Our results and conclusions follow.

2. Data

This study analyzes observations from the Atlantic coast near Duck, North Carolina, on the Outer Banks barrier island (Fig. 1) during 2–18 March 1999 and 11 November–4 December 1999 during the Shoaling Waves Experiment (SHOWEX) (Sun et al. 2001). The roughness elements on the Outer Banks consist of multistory vacation homes and commercial buildings. Despite the short fetch over land due to the narrowness of the Outer Banks, significant mixing is generated near the surface over land due to these large roughness elements and solar heating of the surface.

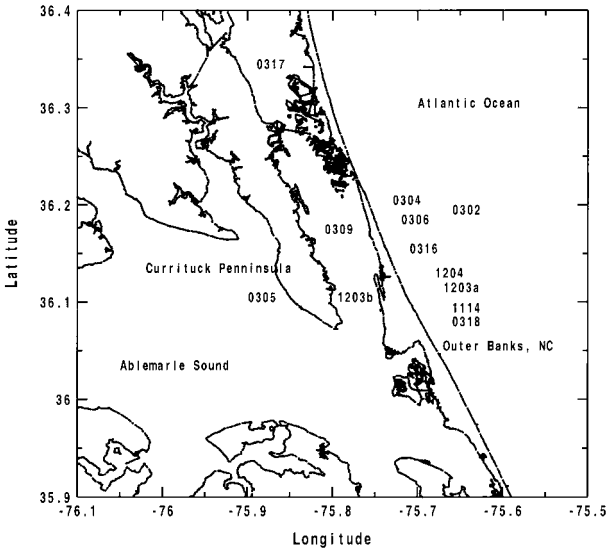

FIG. 1. SHOWEX study area near Duck, NC, and the location and date (mmdd) of the 12 offshore flow case studies. The mean flow is from the SW in all cases except 0305 and 0309 when it is from the NE. The upstream land is the Outer Banks in all cases except 0317, 0305, and 1203b when it is Currituck Peninsula.

The National Oceanic and Atmospheric Administration (NOAA) LongEZ (N3R) aircraft measured the three components of the wind, air temperature, humidity, surface temperature, and atmospheric pressure. With clean aerodynamics and a pusher configuration, the LongEZ is an ideal platform for low-and-slow air surface exchange measurements. The wind components were measured using the BAT turbulence probe designed and built in collaboration with Airborne Research Australia (Crawford and Dobosy 1992). Information from Trimble Advanced Navigation Systems differential Global Positioning System receivers are extended to high frequencies by accelerometers to determine position and platform attitude. The air temperature was measured using a Victory Engineering Corp. microbead thermistor. Surface radiative temperature was measured with an Everest Inter-science Inc. 4000.4GL instrument.

The aircraft flight patterns considered in this work include repeated tracks close to and parallel to the coast for a sequence of offshore distances and heights, as well as repeated tracks perpendicular to the coast for a sequence of different altitudes. The same flight track was flown numerous times to ensure adequate statistics and reduce the random flux sampling errors associated with a single pass of the track. The lowest-level aircraft flights over water were flown between 10 and 20 m.

a. Derived quantities

All derived fields were calculated from quality controlled aircraft flux legs. The original flight legs were first examined to test for the suitability of calculating fluxes with the eddy correlation method. Portions of the leg satisfying criteria for constant altitude and small aircraft roll, pitch, and heading angle changes were considered potential flux legs. The potential flux legs were then subjected to a quality control software package designed to detect and eliminate instrument and data recording problems (Vickers and Mahrt 1997).

Turbulence was defined to include all fluctuations on length scales from 1 km down to the resolution of the instruments (approximately 1 m based on a 50-Hz sampling rate and a typical aircraft ground speed of 50 m s^{-1}). Sensitivity studies testing the length scale dependence of the calculated fluxes showed that a 1-km length scale was sufficient to capture most of the turbulent flux. Derived quantities include the friction velocity, mean wind speed, and TKE:

$$u_{*l} = (\overline{w'u'}^2 + \overline{w'v'}^2)^{1/4}, \quad (1)$$

$$U = (\overline{u}^2 + \overline{v}^2)^{1/2}, \quad \text{and} \quad (2)$$

$$\text{TKE} = 0.5(\overline{u'u'}^2 + \overline{v'v'}^2 + \overline{w'w'}^2), \quad (3)$$

where primes denote fluctuations from a 1-km mean and overbars represent a 1-km average. Here, u_{*l} refers to the local value of the friction velocity at height z.

b. Interpolation method

We interpolate the 1-km data onto a fetch–height (x, z) grid of resolution $\Delta x = 500$ m and $\Delta z = 25$ m with a domain equal to 0–10-km fetch and 10–310 m in height. Fetch is distance over the ocean that an air parcel has traveled since leaving land and is a function of aircraft position, coastal geometry, and wind direction. Quantity ϕ at a grid point was calculated as

$$\phi(x, z) = \frac{\sum w_k \phi_k}{\sum w_k}, \quad (4)$$

where the sum is over all 1-km mean data points and ϕ represents u_{*l}, U, TKE, or the heat flux. The weights (w_k) are assigned inversely proportional to the distance between the observations and the grid point as

$$w_k = \frac{2 - \zeta}{2 + \zeta} \quad \text{and} \quad (5)$$

$$\zeta = \frac{(x_k - x)^2}{X^2} + \frac{(z_k - z)^2}{Z^2}, \quad (6)$$

and we select $X = 3\Delta x$, $Z = 3\Delta z$. For those observations where $|x_k - x| > X$ or $|z_k - z| > Z$, the weight is set to zero; that is, X and Z define a maximum region of influence. The length of time between the first and last aircraft observations included in an individual cross section was approximately 1 h and varied slightly between cases (Table 1). The profile at the coastline ($x = 0$) was calculated as the average of the mean profile over land for the longest land fetches available and the interpolated profile for zero fetch using the segments over the ocean.

TABLE 1. Offshore flow case studies (see Fig. 1 for locations). Mean wind speed, friction velocity, and heat flux are the interpolated values at $x = 0$ (coastline) and $z = 35$ m. Values in parentheses are estimates of the standard error. Asterisks indicate cases with only low-level data.

Date (mmdd)	Time (UTC)	U (m s^{-1})	u_{*l} (m s^{-1})	$\overline{w'\theta'}$ (m s^{-1} °C)
0302	2000	5.7 (0.3)	0.27 (0.04)	0.009 (0.004)
0305	1830	4.5 (0.1)	0.51 (0.03)	0.125 (0.015)
0317	1900	5.0 (0.1)	0.44 (0.02)	0.003 (0.003)
0318	1530	6.5 (0.2)	0.71 (0.02)	0.041 (0.004)
1114	1800	7.1 (0.3)	0.55 (0.02)	0.027 (0.006)
1203a	1330	7.9 (0.3)	0.27 (0.03)	−0.010 (0.012)
1203b	1330	6.0 (0.3)	0.30 (0.06)	−0.014 (0.005)
0304*	1600	12.1 (1.1)	0.46 (0.09)	0.035 (0.013)
0306*	1500	5.7 (0.2)	0.43 (0.03)	0.002 (0.004)
0309*	1530	6.3 (0.3)	0.31 (0.02)	0.020 (0.001)
0316*	1930	4.9 (0.2)	0.45 (0.02)	0.044 (0.011)
1204*	1800	6.2 (0.2)	0.51 (0.02)	0.005 (0.003)

In the interpolation, all information contained in the data was used to extract the spatial structure of the mean. An alternative method, where the data were grouped (binned) into fetch and altitude categories, was employed to obtain the variance, from which we estimated a sampling error. We calculated the standard error for the mean estimates in Table 1 (at $x = 0$ and $z = 35$ m) by combining all observations below 70-m altitude over land and below 50-m altitude over the first 500 m of water fetch. This standard error is an overestimate of the standard error associated with purely random sampling errors due to the unavoidable inclusion of coherent spatial variability in the sample.

The kinematic sea surface momentum flux (u_*^2), which represents the air–sea exchange of momentum, was estimated by linearly extrapolating the interpolated estimates at heights of 10 and 35 m to the surface. In the stable case, where the momentum flux typically increases with height close to the coast, the extrapolation yields an estimate of u_*^2 that is smaller than the estimate at the lowest aircraft measurement height.

c. Residual turbulence timescale

To characterize the residual turbulence that is generated over land and advected over the ocean, we calculate a turbulence timescale. In traditional scaling arguments, the turnover time for a large eddy is proportional to L_s/σ_w, where σ_w is the standard deviation of the vertical wind defined for some suitable averaging time, and L_s is the length scale where 50% of the total variance of the vertical wind occurs at smaller scales. Here, L_s is strongly correlated with the length scale of the peak of the spectra. To estimate L_s, we applied multi-

resolution decomposition (Howell and Mahrt 1997) to the vertical velocity data obtained in the boundary layer over land. The spectra from repeated flight tracks in the same region on the same day were composited by averaging the estimates of L_s for individual passes.

d. Evaluating gradients

The equation of motion for the mean wind is written as

$$\frac{\partial U}{\partial t} + U\frac{\partial U}{\partial x} + W\frac{\partial U}{\partial z} + \frac{\partial \overline{w'u'}}{\partial z} + \frac{\partial \overline{u'u'}}{\partial x} = -\frac{1}{\rho}\frac{\partial P}{\partial x}, \quad (7)$$

where we have neglected terms involving horizontal gradients in the direction parallel to the coast. The terms in Eq. (7) were estimated using finite differences evaluated across a conceptual grid box extending from 1 to 3 km in fetch and from 10 to 135 m in height above the water. Horizontal gradients were computed as the difference of the vertical averages over the grid box, and vertical gradients were computed as the difference of horizontal averages. A sequence of sensitivity studies, where the grid box was moved farther downstream and made larger in the x direction, showed that while the exact magnitude of the terms is sensitive to the region considered, the relative magnitude and sign of the terms are not sensitive. The local time rate of change term ($\partial U/\partial t$) was estimated from the earliest and latest aircraft passes, which were typically 1 h apart.

The mean vertical velocity (W) in the vertical advection term was estimated by first removing the flight-average vertical velocity from the 1-km means. A surprisingly coherent pattern was observed in which the mean vertical motion was downward (upward) in the region of acceleration (deceleration) of the horizontal mean wind. Deceleration of the mean wind and mean rising motion were commonly observed over land, while acceleration of the mean wind and mean sinking motion were found in the first few kilometers downwind from the coast in stable conditions. For the longest sea fetches, the mean vertical motion was small downward.

Attempts to calculate the horizontal pressure gradient by removing the altitude dependence of the pressure as measured by the aircraft were deemed unreliable. As an alternative, we estimated the local horizontal pressure gradient due only to the local horizontal temperature gradient using the hydrostatic equation and the observed temperature field from the aircraft measurements. An estimate of the large-scale horizontal pressure gradient was calculated from the NCEP–NCAR reanalysis surface pressure (Kalnay et al. 1996). The reanalysis is a joint project between the National Centers for Environmental Prediction (NCEP) and the National Center for Atmospheric Research (NCAR). The analyzed surface pressure from the model was interpolated in time and space for each case study.

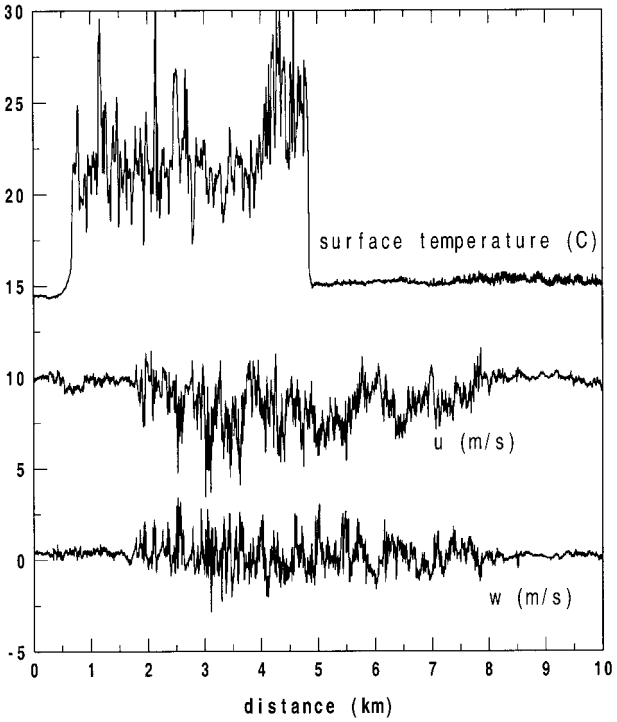

FIG. 2. Surface radiative temperature (°C), horizontal wind speed (m s^{-1}), and vertical wind speed (m s^{-1}) as a function of distance (km) for one aircraft flux leg at 110-m altitude on 1114 as the aircraft travels west to east from over Albemarle Sound (left edge), over the Outer Banks (the warm region), and then over the Atlantic Ocean. The mean flow direction is westerly.

3. Spatial variation

Time series from a single aircraft leg crossing the Outer Banks is shown in Fig. 2. Unlike in the cross sections, in this example the wind components are not time averaged, interpolated, or smoothed. The two coastlines are clearly distinguished by the surface radiative temperature. The stable air–sea temperature difference is 6° to 8°C. The aircraft intersects a convective land-based IBL with strong turbulence at 1.1 km inland from the windward coastline. The turbulence generated over land is advected downwind over the ocean where the wind fluctuations decrease in strength until beyond 4 km, or 8 min travel time, where the turbulence becomes very weak. The 1-km average wind speed is reduced from 10 m s^{-1} over the sound on the windward side of land to 8 m s^{-1} over the leeward side of land. Over the Atlantic, the mean flow accelerates back to its original upstream value by the time that the residual land-based turbulence has collapsed. In the remainder of this section, we discuss case studies of composite fetch–height cross sections in offshore flow (Table 1 and Fig. 1). These case studies provide challenging situations for future attempts to model offshore flow.

Case 0318 (Fig. 3) is downwind of the Outer Banks over the Atlantic, where the air temperature is initially 8°C warmer than the sea surface temperature. Based on

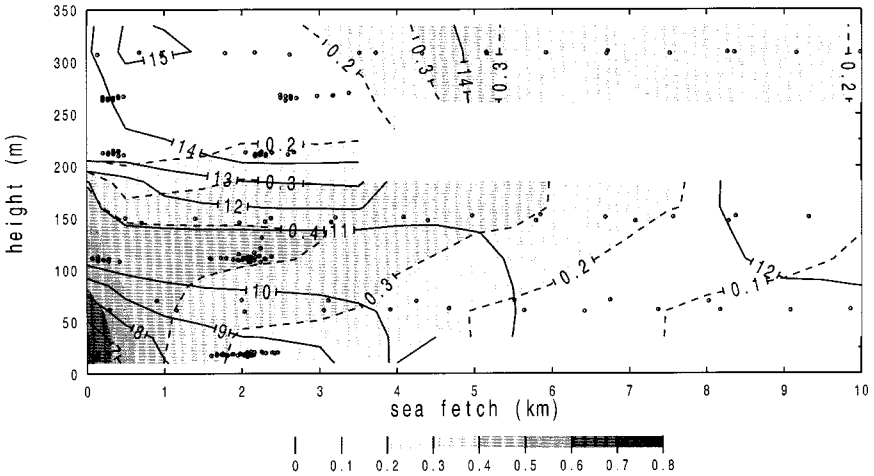

FIG. 3. Fetch–height cross sections for case 0318 of the friction velocity (shaded and dotted contours, m s^{-1}) and the mean wind speed (solid contours, m s^{-1}). Dots indicate locations of the 1-km data points used in the interpolation. Clusters of data points result from the parallel flight tracks.

the decrease in mean TKE with height over land (not shown), the depth of the land-based convective IBL at the leeward coastline after 4.8 km of land fetch is approximately 200 m. Beyond 1 km from the coast, strong residual turbulence advected from land becomes partially detached from the surface leading to a downward momentum flux (and TKE) maxima aloft. Mahrt et al. (2001) observed similar vertical structure of stable offshore flow from tower data off the Danish coast; however, the air–sea temperature difference of the present offshore flow is larger and the vertical structure is more persistent. We attribute the elevated flux maxima to a combination of several factors: (a) more dissipation of the residual turbulence at lower levels due to smaller mean eddy size near the surface, (b) more buoyancy destruction of turbulence at lower levels over the ocean due to the closer proximity to the cold water, and (c) shorter travel time at higher levels, for a given fetch distance, due to the stronger mean wind aloft. Cases 1114 (Fig. 4) and 0317 (Fig. 5) are similar in many respects to case 0318. In all three of these stable offshore flow cases, an elevated layer of momentum flux and TKE maxima is observed along with acceleration of the low-level mean wind in the first several kilometers over the water.

In case 1203a, a shallow (<50-m depth) convective IBL develops over the Atlantic in response to cold air advection from land. The air is 3°C colder than the water. Beyond 1 km from the coast, the sea surface momentum flux is constant with fetch and the momentum flux slowly decreases with height (Fig. 6). This unstable case is quite different from the stable case, which included a rapid decrease in the sea surface momentum flux with fetch, an increase in the momentum flux with height, and acceleration of the low-level mean wind.

The remaining case studies (not shown) clearly demonstrate the strong influence of stability (air–sea temperature difference) on the fetch dependence of the sea surface momentum flux. For unstable conditions, in which buoyancy generation of turbulence over the warm water is significant, the sea surface momentum flux is nearly independent of fetch beyond the first kilometer offshore. For stable flow of warm air over cool water, the momentum flux decreases rapidly in the first several kilometers and gradually approaches a constant value after 6–10 km of fetch.

4. Advective-decay timescale

In this section, we test a prediction for the travel-time dependence of the sea surface momentum flux based on a characteristic timescale of the turbulence in the upstream boundary layer over land. The hypothesis is that local generation of momentum flux over the ocean for short fetch is small compared to the influence due to advection of strong turbulence from land in stable offshore flow. Cases with convective conditions over the water, where local buoyancy generation of turbulence is significant, were excluded.

We calculated an advective-decay rate that describes the observed decrease in the sea surface momentum flux with increasing travel time from the coast. From a Lagrangian viewpoint, the advective-decay rate in stable offshore flow is at least partly due to viscous dissipation of the Reynolds stress. Based on the actual travel-time dependence (Fig. 7), we formulated the sea surface momentum flux as a function of travel time t from the coast as

$$u_*^2(t) = u_{*o}^2 \exp(-t/\tau) + u_{*\mathrm{eq}}^2[1 - \exp(-t/\tau)], \quad (8)$$

where τ is the advective-decay timescale, $u_{*\mathrm{eq}}$ is the equilibrium value of u_* for long travel time over the water beyond the influence of advection from land, and

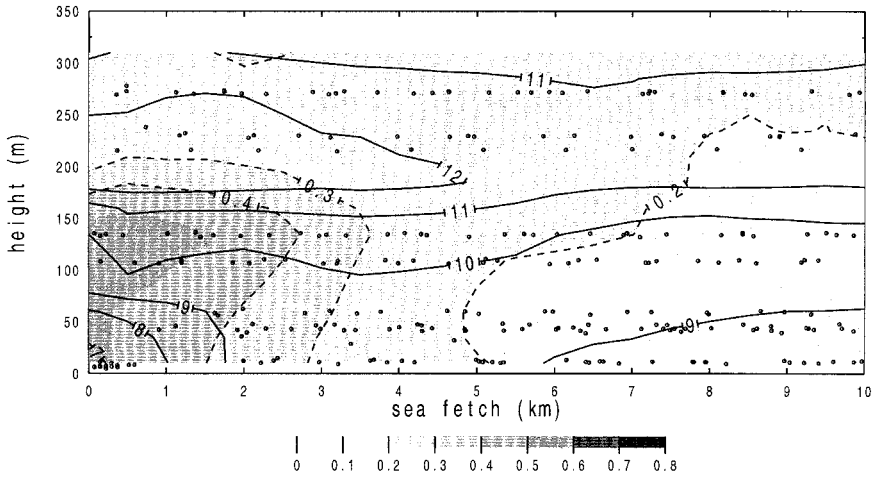

FIG. 4. Same as Fig. 3 except for case 1114.

u_{*o} is the initial value at the coast. The timescale τ was calculated for each case study by applying linear least squares regression to the $u_*^2(t)$ values over the ocean, of which there is one estimate every 500 m of fetch.

An independent predictor for the advective-decay timescale that is based only on the vertical velocity fluctuations in the upstream boundary layer over land is

$$\tau_L = (L_s + c)/\sigma_w, \tag{9}$$

where L_s is the eddy length scale for the turbulence in the land-based boundary layer based on the vertical velocity spectra (section 2), σ_w is the standard deviation of the vertical velocity in the land-based boundary layer, and c is a constant that crudely compensates for influences other than decay. The formulation for τ_L is analogous to traditional theory for dissipation of turbulence variances, where the dissipation timescale increases with the characteristic length scale of the eddies and decreases with the strength of the mixing. If decay of advected turbulence dominates the sea surface momentum flux in stable offshore flow, τ_L should be related to timescale τ.

We find that the timescale τ, which represents the observed rate of decrease in the sea surface momentum flux [Eq. (8)], and the predictor timescale τ_L are indeed related (Fig. 8). That is, the spatial structure of the sea surface momentum flux depends on the characteristics of the turbulence in the upstream boundary layer over land. This implies that advection and decay processes primarily determine the air–sea momentum exchange. Using an alternate eddy length scale for the turbulence in the land-based boundary layer equal to L_s plus a constant [$c = 70$ *m* in Eq. (9)] in evaluating τ_L leads to a linear one-to-one relationship between τ and τ_L (plus signs in Fig. 8). One interpretation of $c > 0$ is that the turbulence is not in pure decay and that generation of turbulence over the water is not negligible. Using $c > 0$ effectively increases L_s and slows the net rate of decay.

5. Momentum budget

Horizontal advection is the largest term close to the coast (Table 2) in the equation of motion for the offshore mean wind [Eq. 7] due to acceleration (deceleration in unstable case) of the mean wind and due to the generally strong wind speeds. An increase in the low-level mean wind speed in the first several kilometers offshore is associated with an increase in the downward momentum flux with height and with mean sinking motion. Vertical

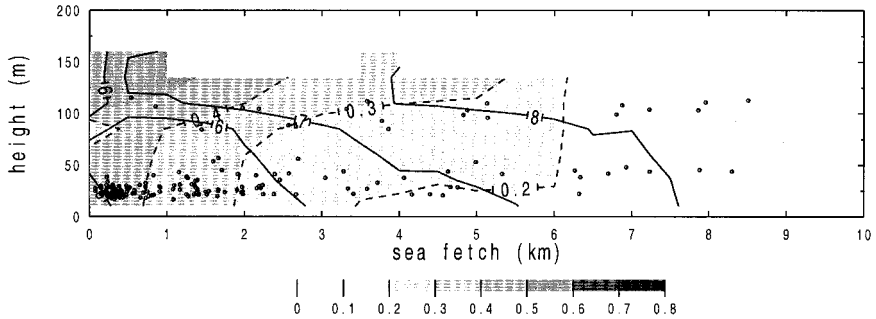

FIG. 5. Same as Fig. 3 except for case 0317.

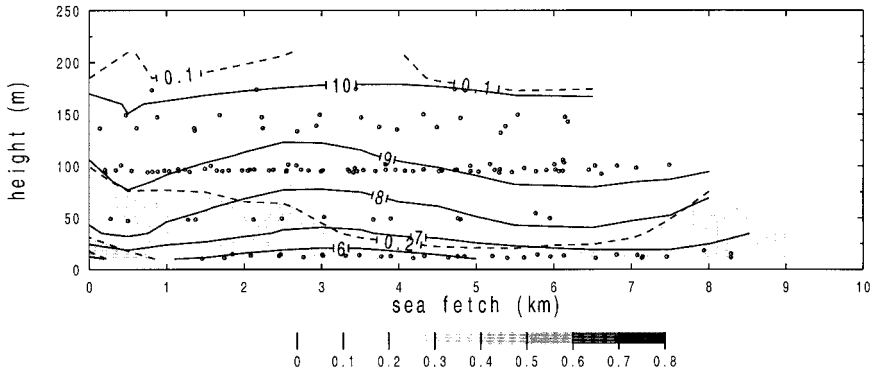

FIG. 6. Same as Fig. 3 except for case 1203a.

advection brings stronger momentum down toward the surface since the mean wind speed increases with height. The three cases with these characteristics (0318, 1114, and 0317) are stable flow of warm air over cooler water. The case with flow of cool air over warm water (1203a in Table 2) is associated with deceleration of the mean wind, a decrease in the momentum flux with height, and mean rising motion. The statistical uncertainty in the magnitude of the horizontal advection and vertical flux divergence terms is 20% or less. The remaining terms are less certain (Table 2).

The hydrostatic part of the horizontal pressure gradient due to the local horizontal temperature gradient is small compared to the residual pressure gradient (the gradient required for balance) except in the unstable case (1203a in Table 2). In this unstable case, they are approximately equal and Eq. (7) is nearly balanced. The large-scale horizontal pressure gradient from the reanalysis model (-0.49 m s^{-1} per hour) is small in this unstable case. In the three stable cases, the large-scale reanalysis pressure gradient has the same sign and approximately the same magnitude as both the vertical advection and the vertical flux divergence terms. These large-scale pressure gradients are of the correct sign to help balance local horizontal advection but significant residual remains in the budget for cases 0318 and 1114. The local momentum budget inbalance as a percentage of the horizontal advection term when using the large-scale pressure gradient is 30%, 53%, and 2% for the stable cases 0318, 1114, and 0317, respectively.

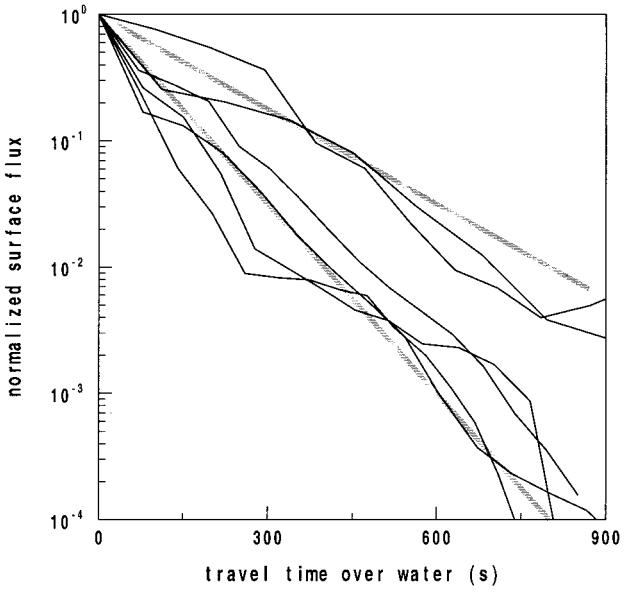

FIG. 7. Decrease in the normalized sea surface momentum flux $(u_*^2(t) - u_{*eq}^2)/(u_{*o}^2 - u_{*eq}^2)$ vs travel time over the water (t). The two heavy lines are the predicted decrease from Eq. (8) for values of the advective-decay timescale τ equal to 200 s (lower line) and 400 s (upper line).

6. Conclusions

Aircraft measurements taken during offshore flow near a barrier island on the east coast of the United States during the Shoaling Waves Experiment have been examined. For stable flow of warm air over cool water, the sea surface momentum flux decreases rapidly with increasing fetch for the first few kilometers offshore and gradually reaches equilibrium values 10 km offshore. The observed decrease in the sea surface momentum flux with travel time from the coast is predicted using a characteristic timescale of the turbulence in the upstream boundary layer over land. This suggests that, close to the coast, advection and decay of residual turbulence strongly influence the air–sea momentum exchange. In this case, similarity theory is not adequate to predict the flux due to dependence on upstream conditions.

With flow of stable warm air over cool water, the residual turbulence advected from land becomes partially detached from the sea surface leading to a momentum flux and turbulence energy maxima aloft. Contrary to the usual concept of a boundary layer, the downward momentum flux increases with height. This is due to a combination of stronger dissipation of the advected turbulence at lower levels and less travel time available

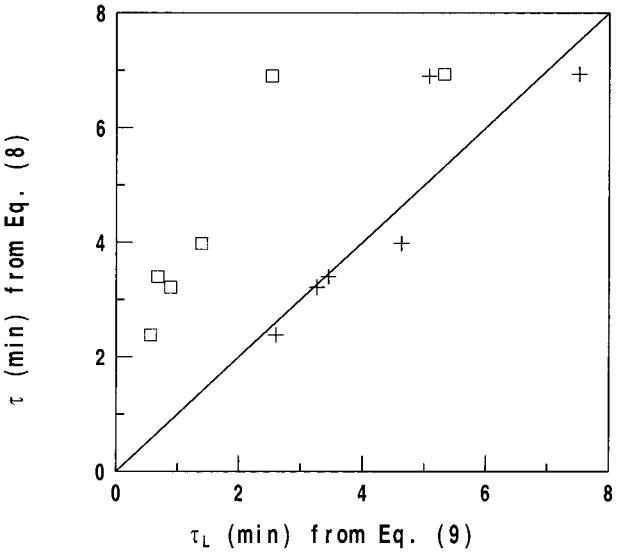

FIG. 8. Advective-decay timescale τ based on observed decrease in u_*^2 with travel time [Eq. (8)] vs τ_L calculated from characteristics of the upstream land-based boundary layer [Eq. (9) with $c = 0$] for six different case studies (squares). The plus signs show τ vs τ_L using $c = 70$ m in calculating τ_L.

for decay at higher levels due to the increase in the mean wind with height.

With flow of unstable cool air over warm water, advection and decay of residual turbulence also occur. However, the relative contribution to the total turbulence level is less due to buoyancy generation of turbulence over the ocean. Unlike the stable case, the sea surface momentum flux for unstable flows is relatively invariant with fetch or travel time. In the unstable case, the momentum flux decreases with height as in traditional boundary layers.

Estimates of the individual terms in the equation of motion for the offshore mean wind show that horizontal advection is the largest term. The vertical advection term, the vertical flux divergence term, and the horizontal pressure gradient term all act to balance horizontal advection. Acceleration (deceleration) of the mean flow in the first few kilometers offshore is associated with an increase (decrease) in the downward momentum flux with height and mean sinking (rising) motion.

Acknowledgments. We thank the NOAA LongEZ group for the field support. The useful comments of the reviewers are greatly appreciated. This work was supported by the Office of Naval Research under Grant N00014-97-1-0279.

REFERENCES

Banner, M. L., 1990: The influence of wave breaking on the pressure distribution in wind–wave interactions. *J. Fluid Mech.,* **211,** 463–495.

Crawford, T. L., and R. J. Dobosy, 1992: A sensitive fast-response probe to measure turbulence and heat flux from any airplane. *Bound.-Layer Meteor.,* **59,** 257–278.

Donelan, M. A., 1990: Air–sea interaction. *Ocean Engineering Science,* B. LeMehaute and D. M. Hanes, Eds., John Wiley and Sons, 239–292.

Fairall, C. W., E. F. Bradley, D. P. Rogers, J. B. Edson, and G. S. Young, 1996: Bulk parameterization of air–sea fluxes for Tropical Ocean-Global Atmosphere Coupled-Ocean Atmosphere Response Experiment. *J. Geophys. Res.,* **101,** 3747–3764.

Garratt, J. R., 1990: The internal boundary layer—A review. *Bound.-Layer Meteor.,* **50,** 171–203.

Geernaert, G. L., S. E. Larsen, and F. Hansen, 1987: Measurements of the wind stress, heat flux and turbulence intensity during storm conditions over the North Sea. *J. Geophys. Res.,* **92,** 127–139.

Högström, U., 1996: Review of some basic characteristics of the atmospheric surface layer. *Bound.-Layer Meteor.,* **78,** 215–246.

Horst, T. W., and J. C. Weil, 1994: How far is far enough? The fetch requirements for micrometeorological measurements of surface fluxes. *J. Atmos. Oceanic Technol.,* **11,** 1018–1025.

Howell, J. F., and L. Mahrt, 1997: Multiresolution flux decomposition. *Bound.-Layer Meteor.,* **83,** 117–137.

Kalnay, E., and Coauthors, 1996: The NCEP/NCAR 40-Year Reanalysis Project. *Bull. Amer. Meteor. Soc.,* **77,** 437–471.

Mahrt, L., D. Vickers, J. B. Edson, J. M. Wilczak, and J. Hare, 2001: Boundary-layer transitions in offshore flow. *Bound.-Layer Meteor.,* in press.

Monin, A. S., and A. M. Yaglom, 1975: *Statistical Fluid Mechanics: Mechanics of Turbulence.* MIT Press, 769 pp.

Nieuwstadt, F., and R. Brost, 1986: The decay of convective turbulence. *J. Atmos. Sci.,* **43,** 532–546.

Smedman, A.-S., M. Tjernström, and U. Högström, 1993: Analysis of the turbulence structure of a marine low-level jet. *Bound.-Layer Meteor.,* **66,** 105–126.

Sorbjan, Z., 1997: Decay of convective turbulence revisited. *Bound.-Layer Meteor.,* **82,** 501–515.

Sun, J., D. Vandemark, L. Mahrt, D. Vickers, T. L. Crawford, and C. Vogel, 2001: Momentum transfer over the coastal zone. *J. Geophys. Res.,* in press.

Vickers, D., and L. Mahrt, 1997: Quality control and flux sampling problems for tower and aircraft data. *J. Atmos. Oceanic Technol.,* **14,** 512–526.

TABLE 2. Terms in the equation of motion for different case studies in units of m s^{-1} per hour. The horizontal pressure gradient term was calculated as a residual from the equation of motion. Values in parentheses are estimates of the standard error.

Date (mmdd)	$\partial U/\partial t$	$U\partial U/\partial x$	$W\partial U/\partial z$	$\partial\overline{w'u'}/\partial z$	$\partial\overline{u'u'}/\partial x$	$\frac{1}{\rho}\partial P/\partial x$
0318	0.9 (0.4)	8.1 (0.4)	−1.6 (0.7)	−2.3 (0.4)	−0.5 (0.1)	−4.7
1114	0.7 (0.6)	13.7 (0.9)	−1.5 (0.9)	−2.4 (0.3)	−0.7 (0.2)	−9.9
0317	1.3 (0.7)	8.7 (0.3)	−3.9 (1.1)	−3.3 (0.5)	−0.6 (0.1)	−2.2
1203a	0.2 (0.6)	−8.4 (1.1)	3.3 (1.2)	1.1 (0.2)	−0.1 (0.1)	3.9